

MULTIPLE PION AND KAON PRODUCTION IN HIGH-ENERGY  
NUCLEUS-NUCLEUS COLLISIONS: MEASUREMENTS VERSUS SPECIFIC  
MODELS

P. GUPTAROY<sup>a, 1</sup>, BHASKAR DE<sup>b, i</sup>, S. BHATTACHARYYA<sup>b, j</sup>  
and D. P. BHATTACHARYYA<sup>a, k</sup>

<sup>a</sup>*Department of Theoretical Physics, Indian Association for the Cultivation of Science,  
Kolkata-700032, India*

<sup>b</sup>*Physics and Applied Mathematics Unit (PAMU), Indian Statistical Institute,  
Kolkata-700108, India*

*E-mail addresses:* <sup>i</sup>*bhaskar\_r@www.isical.ac.in*, <sup>j</sup>*bsubrata@www.isical.ac.in*,  
<sup>k</sup>*tpdpb@mahendra.iacs.res.in*

Received 17 October 2001; revised manuscript received 18 January 2002

Accepted 27 May 2002      Online 7 February 2003

The pion and kaon rapidity densities and the nature of kaon-pion ratios offer two very prominent and crucial physical observables on which modestly sufficient data for heavy nucleus collisions are available to date. In the light of two sets of models – one purely phenomenological and the other with a modest degree of a dynamical basis – we try to examine the state of agreement between calculations and experimental results obtainable from the past and the latest measurements. Impact and implications of all these would also finally be spelt out.

PACS numbers: 25.75.-q, 13.85.Ni, 12.38.Mh

UDC 529.126

Keywords: relativistic heavy ion collisions, inclusive production, quark gluon plasma

## 1. Introduction

Multiparticle production in both high-energy nuclear and particle collisions is still a mystery, in so far as the understanding of the dynamics of the production of secondaries, especially of the soft varieties, is concerned. Of the various types of particles produced, mesons, especially the  $\pi$ -mesons, constitute, in practical terms, the near totality of the secondaries. We would concentrate here only on two important production characteristics of  $\pi$ -mesons (pions) and of K-mesons

---

<sup>1</sup>On leave from Department of Physics, Raghunathpur College, P.O.: Raghunathpur 723133, Dist. Purulia (WB), India.

(kaons) in some nucleus-nucleus collisions. Kaons are also important because of their strangeness content and because they are supposedly related with the physics of the postulated quark-gluon plasma (QGP) signatures [1]. Secondly, kaons are the lightest variety of the measurable strange particles. Lastly, kaon production is considered to have a bearing on the nuclear equation of state [2]. In fact, our interest to take up these problems was further arisen and intensified by a very recent study of inclusive production of particles in nucleus-nucleus collisions by Kahana and Kahana [3]. The work is, thus, to be viewed as an appropriate response to the stimulus received from Ref. [3].

In our work here, we confine ourselves to the investigations of the two very fundamental observables, viz, the rapidity-density behaviour and the nature of the kaon-pion ratios. Of these two, the former for production of the charged secondaries (which are mostly pions at relativistic energy) reflects among other things the dynamical range of the interaction (from the width factor) and some other relevant physical facts related with the emission of the particles. The changes in the peak position of the rapidity spectra presented by the rapidity-density vs. rapidity graphs might reveal some predicted aspects of collective phenomena in high energy collisions, throw light on the multiplicity behaviour and also have relevance for estimation of the energy density during the collision [4]. All these factors have some relationship with the proposed QGP diagnostics and some obvious implications for understanding the nature of cosmic ray interactions at superhigh energies. The latter observable has also significance for both conjectured QGP signatures and some cosmic-ray physics problems of a somewhat complex nature.

The organisation of the paper is as follows: In Sect. 2, we provide brief outlines of the models chosen for this study. In Sect. 3, the results obtained by the model-based calculations are presented mostly diagrammatically. In Sect. 5, we sum up the most important conclusions which come as a natural follow-up from the preceding chapter (Sect. 4), containing fairly detailed discussion on the results and the observations made in Sect. 3.

## 2. *The approaches*

In the present work, we will make use of two sets of theoretical models to interpret some of the latest and topical observables which were measured and reported by various groups like NA49, NA35, E802 collaboration etc. [5-8] in the recent past. The first set has a modest degree of dynamical basis and some prior check-ups with data. It is called here as the sequential chain model (SCM). The second set consists of two models which are of purely phenomenological character. They are the De-Bhattacharyya model (DBM), which is still in its infancy, and the other is the hadronic string dynamics (HSD) model or approach which is also in the budding stage. In what follows, we present brief sketches of the models.

### 2.1. *The sequential chain model (SCM)*

Here, a particular version of the sequential chain model (SCM) [9] is used. In this model, the expressions are derived on the basis of the field theoretical

considerations for the inclusive cross sections and average multiplicities for various types of secondary pions (of any variety), kaons (of each type) in the reaction of type  $p + p \rightarrow c + x$  and they are given by the following set of relations.

For any variety of secondary pions ( $\pi^+$ ,  $\pi^-$  or  $\pi^0$ ), the expression for the inclusive cross section is derived on the basis of field-theoretical consideration and the application of the Feynman diagram technique. For negative pions, this is given by the following expression,

$$E \frac{d^3\sigma}{dp^3} \Big|_{pp \rightarrow \pi^- x} \cong C_{\pi^-} \exp\left(\frac{-26.88 p_T^2}{\langle n_{\pi^-} \rangle (1-x)}\right) \times \exp(-2.38 \langle n_{\pi^-} \rangle x), \quad (1)$$

where  $|C_\pi|$  is interaction-specific and could be different for different energy regions as well with,

$$\langle n_{\pi^+} \rangle_{pp} \cong \langle n_{\pi^-} \rangle_{pp} \cong \langle n_{\pi^0} \rangle_{pp} \cong 1.1 s^{1/5}. \quad (2)$$

For any energy and low  $p_T$ , one assumes reasonably

$$E \frac{d^3\sigma}{dp^3} \Big|_{pp \rightarrow \pi^- x} \cong E \frac{d^3\sigma}{dp^3} \Big|_{pp \rightarrow \pi^+ x} \cong E \frac{d^3\sigma}{dp^3} \Big|_{pp \rightarrow \pi^0 x}. \quad (3)$$

Similarly, for kaons of any specific variety ( $K^+$ ,  $K^-$ ,  $K^0$  or  $\bar{K}^0$ ), we have

$$E \frac{d^3\sigma}{dp^3} \Big|_{pp \rightarrow K^- x} \cong C_{K^-} \exp\left(\frac{-1.329 p_T^2}{\langle n_{K^-} \rangle^{3/2}}\right) \times \exp(-6.55 \langle n_{K^-} \rangle x), \quad (4)$$

with  $|C_{K^-}|$  having traits similar to that  $C_\pi$ , and

$$\langle n_{K^+} \rangle_{pp} \cong \langle n_{K^-} \rangle_{pp} \cong \langle n_{K^0} \rangle_{pp} \cong \langle n_{\bar{K}^0} \rangle_{pp} \cong 5 \times 10^{-2} s^{1/4}. \quad (5)$$

And at low  $p_T$

$$E \frac{d^3\sigma}{dp^3} \Big|_{pp \rightarrow K^- x} \cong E \frac{d^3\sigma}{dp^3} \Big|_{pp \rightarrow K^+ x} \cong E \frac{d^3\sigma}{dp^3} \Big|_{pp \rightarrow K^0 x \text{ or } \bar{K}^0 x}. \quad (6)$$

The term rapidity distribution plays another key role to address some other salient features of the reaction dynamics and the properties of the production of the secondary particles. The rapidity distribution for the secondaries in  $p + p \rightarrow c + x$  types of reactions is derived from the inclusive production cross sections. The steps are like these:

(i) from  $[E d^3\sigma/dp^3]_{pp}$  to  $[d\sigma/dy]_{pp}$  we have

$$\frac{d\sigma}{dy} \Big|_{pp} = 2\pi \int [E \frac{d^3\sigma}{dp^3}]_{pp} d^2p_T, \quad (7)$$

and (ii) from  $[d\sigma/dy]_{pp}$  to  $[dN/dy]_{pp}$  there is another relation, viz.,

$$\frac{dN}{dy} \Big|_{pp} = \frac{1}{\sigma_{inel}} \frac{d\sigma}{dy} \Big|_{pp}. \quad (8)$$

For the case of pions the rapidity distribution would now become

$$\frac{dN}{dy} \Big|_{pp \rightarrow \pi x} = 50.375 s^{1/5} \exp(-5.28 s^{-0.3} m_T \sinh y_{cm}), \quad (9)$$

and for the case of kaons, the relation now simply becomes

$$\frac{dN}{dy} \Big|_{pp \rightarrow Kx} = 13.06 s^{3/8} \exp(-0.655 s^{-0.25} m_T \sinh y_{cm}). \quad (10)$$

From nucleon – nucleon to nucleus – nucleus collisions, we would like to use here a standard connector prescribed by Wong [10]. The method is shown in the Appendix.

### 2.2. Hadron/nucleus–nucleus collisions: a new phenomenological model

Very recently, De and Bhattacharyya [11,12] checked and forwarded a phenomenological fit to the rapidity density for the production of pions in a host of nucleus – nucleus collisions at high energies in the following manner:

$$\frac{dN}{dy} \Big|_{AB} = (A.B)^{f(y)} \frac{dN}{dy} \Big|_{pp}, \quad (11)$$

where

$$f(y) = \alpha + \beta y + \gamma y^2, \quad (12)$$

with some reaction-specific values for  $\alpha$ ,  $\beta$ ,  $\gamma$  which we will present here for some specific reactions. The exponent in the mass-number dependence could also be expressed in a quadratic form in terms of the transverse momentum ( $p_T$ ) of the secondary detected in a specific nuclear collision. And this new parametrisation of mass-number dependence is here loosely referred to as the De-Bhattacharyya model (DBM). The chosen form of  $dN/dy|_{pp}$  in expression (11) above is given by

$$\frac{dN}{dy} \Big|_{pp} = C [1 + \exp(\frac{y - y_0}{\Delta})]^{-1}, \quad (13)$$

where the letters (symbols) have their contextual significance and meaning; their values for the calculational purposes were obtained from Thome et al. [13]. The expression (13) is, quite obviously, valid for pp (and  $p\bar{p}$ ) collisions. The point now is to adopt this form with suitable values of  $C$  and  $y_0$  parameters for various nucleon-nucleus and nucleus-nucleus collisions at high energies. In order to proceed along this line most reasonably we need to study at the very beginning the  $\sqrt{s}_{NN}$  dependence of  $C$  and  $y_0$ , for which we introduced some phenomenological generalised expressions describing their physical nature [12]. The graphical plots on two sets of variables –  $C$  vs.  $\sqrt{s}$  and  $y_0$  vs.  $\sqrt{s}$  are made on the basis of them (not shown here and given in Ref. [12]). For a specific nucleon-nucleus (or nucleus-nucleus) collisions at high energies, we obtain the useable values of  $C$  and  $y_0$  from the two graphs, as soon as the  $\sqrt{s}_{NN}$  for the specific interaction is known or given in the data sets.

### 2.3. *The hadron string dynamics (HSD) approach*

In the HSD approach [14], the high-energy inelastic hadron-hadron collisions are described by the Fritiof model, where two incoming hadrons do emerge from the reaction as two excited colour-singlet states, i.e. strings. The energy and momentum transfer in this model are assumed to happen instantaneously at the collision time. With the phenomenological description of the soft processes, the global properties of heavy-ion collisions could be described satisfactorily, as stated by Geiss et al. [14]. The HSD approach serves data on energy dependent cross-section in complete regime for the various prong cross-sections of pp interactions. The particle production from the Fritiof model has also the merit of producing good fit to the inelastic proton-proton (baryon-baryon) collisions from SPS energies to the string threshold,  $\sqrt{s} = 2.65$  GeV.

The contribution of the string-fragmentation model and the covariant transport theory implies the use of a time scale for the particle production process, i.e., the formation time ( $t_f$ ). This includes the formation of the string, the fission of the string due to single and multiple quark-antiquark production into small substrings and also the time to form finally physically observable hadrons. It can be interpreted as the time needed for a hadron to tunnel out of the vacuum and to form its internal wave function. In the HSD model, the formation time is a single fixed parameter for all hadrons and is set to  $t_f = 0.8$  fm/c in the rest frame of the new produced particle. In the c.m. of a string, there are some separate stipulations for the final freeze-out. The model produces modestly good results for some observables; but it has its own complications and phenomenological features as well. This procedure does essentially lead only to "heuristic approximation of the underlying soft partonic dynamics.." [14]. For the strangeness production, in particular, the model has to take into account the meson rescattering and reabsorption processes [14]. In explaining the features of the strangeness production, this is a compulsion for and a constraint on the HSD approach. In fact, this is somewhat an intrinsic characteristics of this model. And with incorporations of all this, it is claimed that kaon production in nucleon-nucleon collisions could be accommodated within the HSD approach over many order of magnitude. But, for the nucleus-nucleus collisions, this approach does not offer very promising results, as we find in this study. For presenting the results obtained on the basis of this approach either in the tables or in the figures, we have relied here mainly on Geiss et al. [14].

## 3. *The results*

Now let us proceed to apply the chosen models to interpret some recent experimental results reported by various groups. Here, the main observables are the rapidity densities and the kaon-pion ratios which would come under purview of the scrutiny of the present work.

### 3.1. *Rapidity densities of secondary pions*

With a view to applying the DBM to explain data, we present the values of the parameters  $\alpha$ ,  $\beta$  and  $\gamma$  of DBM (Eq.(12)) for different reactions like p + S, p + Au,

S + S, S + Au, Pb + Pb etc. at SPS energies. They are given in Table 1. Thereafter, in Table 2, we compare the rapidity-density values for various collisions obtained on the basis of the different models that are applied here. Moreover, the figures

TABLE 1. Values of  $\alpha$ ,  $\beta$  and  $\gamma$  for different interactions in DBM.

Collision	$E$ (GeV)	$\alpha$	$\beta$	$\gamma$	$\frac{\chi^2}{\text{ndf}}$
p+S	200	$0.048 \pm 0.010$	$-0.011 \pm 0.007$	$-0.034 \pm 0.007$	0.615
p+Au	200	$0.104 \pm 0.003$	$-0.01 \pm 0.003$	0	0.226
S+S	200A	$0.45 \pm 0.005$	$-0.033 \pm 0.004$	$-0.008 \pm 0.002$	1.001
S+Ag	200A	$0.446 \pm 0.001$	$-0.005 \pm 0.001$	$-0.016 \pm 0.001$	1.529
S+Au	200A	$0.412 \pm 0.018$	$-0.028 \pm 0.0003$	$-0.018 \pm 0.001$	0.193
Pb+Pb	160A	$0.452 \pm 0.001$	$-0.013 \pm 0.001$	$-0.02 \pm 0.0003$	0.251

TABLE 2. Comparison of rapidity distribution of pions for various interactions in the range  $3 < y < 4$ . First five sets of data are from NA35 Collaboration [7] and the last one is from NA49 Collaboration [6]. Theoretical fits are based on the SCM, the DBM and the HSD.

Systems	$\frac{dN}{dy}   \pi$   data	$\frac{dN}{dy}   \pi$   SCM	$\frac{dN}{dy}   \pi$   DBM	$\frac{dN}{dy}   \pi$   HSD
p+S	$1.3 \pm 0.2$	1.29	1.40	1.48
p+Au	$1.6 \pm 0.1$	1.91	2.32	2.58
S+S	$25 \pm 1$	31	25.75	25.60
S+Ag	$40 \pm 2$	44	46.62	46.88
S+Au	$47 \pm 5$	45	44.84	50.5
Pb+Pb	$150 \pm 1$	150.6	156	165.1

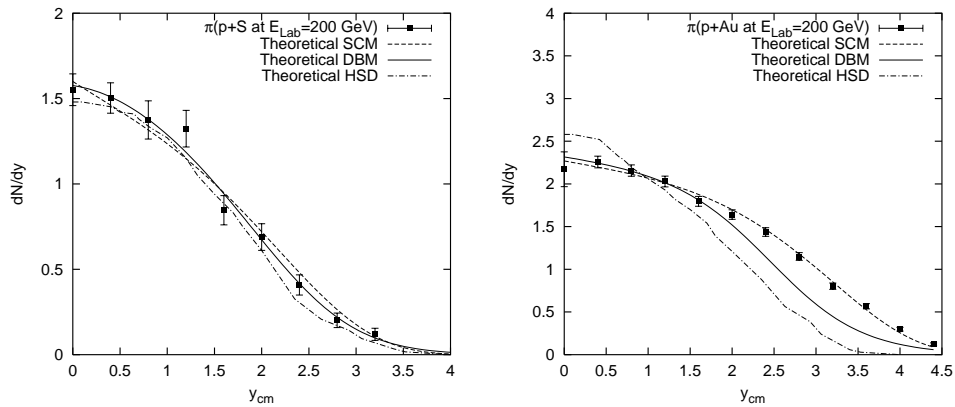


Fig. 1. Rapidity distribution for charged pions in central p + S collisions at 200 AGeV/c [7,14]. The lines show the results of SCM, DBM and HSD model.

Fig. 2 (right). Rapidity distribution for charged pions in central p + Au collisions at 200 AGeV/c [7,14]. The lines show the results of SCM, DBM and HSD model.

(Figs. 1 to 6) present the rapidity distributions of pions for the above collisions at SPS energies done theoretically by the SCM, the DBM and the HSD against the experimental results.

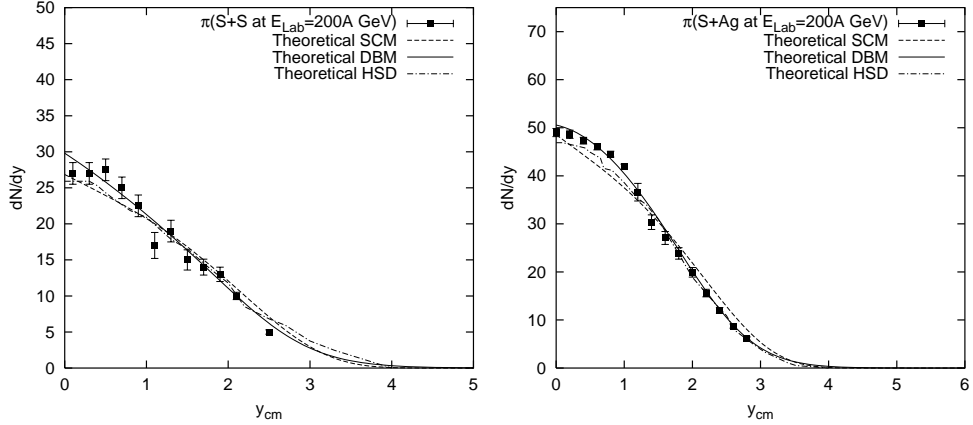


Fig. 3. Presentation of plot of the rapidity distribution of pions for S + S collisions for various values of  $y$ , the rapidity variable. The lines are based on the results of SCM, DBM and HSD model against the obtained data sets [7,14].

Fig. 4 (right). Rapidity distribution for charged pions in central S + Ag collisions at 200 AGeV/c [7,14]. The lines show the results of SCM, DBM and HSD model.

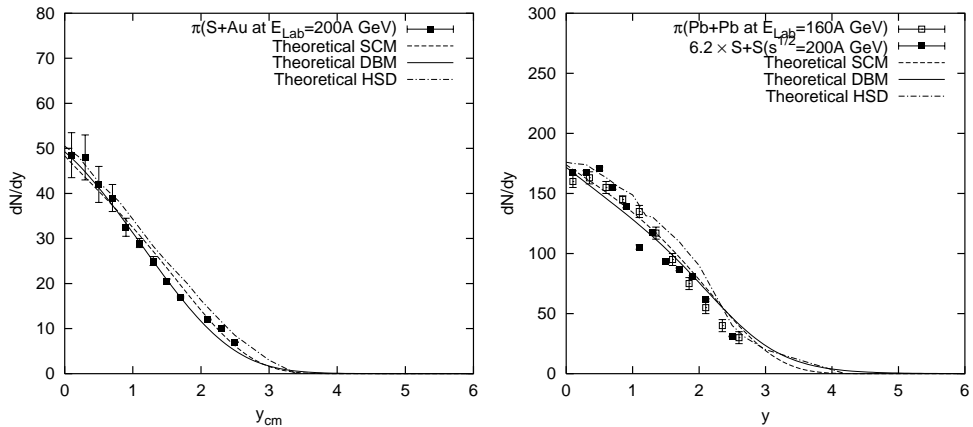


Fig. 5. Presentation of plot of the rapidity distribution of pions for S + Au collisions for various  $y$  at 200 AGeV/c. The lines are based on the results of SCM, DBM and HSD model against the obtained data sets [7,14].

Fig. 6 (right). Presentation of the plot of the rapidity distributions of pions for Pb + Pb and S + S collisions for various values of  $y$ , the rapidity variable. The results of SCM, DBM and HSD approach are shown by the lines against the obtained data sets [6,14].

### 3.2. Rapidity-densities of secondary kaons

Kaons are produced in four varieties: positively charged ( $K^+$ ), negatively charged ( $K^-$ ), and neutral  $K^0$  and  $\bar{K}^0$  mesons. We are interested here only in the charged varieties. We would apply all three models to obtain the results for explaining the data on  $K^+$  and  $K^-$  meson production in recent high-energy heavy-ion experiments. In doing so, a few model-dependent features are to be presented first.

According to the SCM, positive particle production takes place in two steps. The first component of it originates from statistical equal probability of production of any variety of K-mesons. But for  $\pi^+$ ,  $K^+$  and p (secondary proton) production, SCM proposed [9a] some additional modes of excess production which was generalised as the nature's favouritism to positive particles. While treating data in the SCM-dependent way, one has to use in final calculations the following form of relation

$$\left[\frac{dN}{dy}\right]^{K^+} \simeq [1 + Cp_T^{K^+}] \left[\frac{dN}{dy}\right]^{K^-} \quad (14)$$

wherein the production term in the right-hand side is derived from the rigorous field-theoretic considerations and the above-given simplified form is arrived at by some natural high-energy assumptions and approximations.

Hereafter, let us put forward the values of the parameters  $\alpha$ ,  $\beta$  and  $\gamma$  in connection with the DBM for production of  $K^+$  and  $K^-$  in different nuclear reactions, particularly in Pb + Pb at SPS energies and in p + Be, p + Au and Au + Au collisions at AGS energies. The values of the three parameters are given in Table 3 and Table 4.

TABLE 3. Values of  $\alpha$ ,  $\beta$  and  $\gamma$  for the  $K^+$  production in different interactions in DBM.

Collision	$E$ (GeV)	$\alpha$	$\beta$	$\gamma$	$\frac{\chi^2}{\text{ndf}}$
Pb+Pb	160A	$0.76 \pm 0.001$	$0.02 \pm 0.001$	$-0.02 \pm 0.01$	1.664
p+Be	14.6	$0.65 \pm 0.02$	$0.02 \pm 0.01$	$0.09 \pm 0.02$	0.190
p+Au	14.6	$0.38 \pm 0.01$	$0.02 \pm 0.01$	$0.04 \pm 0.01$	1.343
Au+Au	11.6A	$0.641 \pm 0.002$	$0.012 \pm 0.005$	$-0.160 \pm 0.002$	1.472

TABLE 4. Values of  $\alpha$ ,  $\beta$  and  $\gamma$  for the  $K^-$  production in different interactions in DBM.

Collision	$E$ (GeV)	$\alpha$	$\beta$	$\gamma$	$\frac{\chi^2}{\text{ndf}}$
Pb+Pb	160A	$0.71 \pm 0.001$	$0.07 \pm 0.01$	$-0.16 \pm 0.02$	2.372
p+Be	14.6	$0.08 \pm 0.04$	$0.5 \pm 0.3$	$0.3 \pm 0.1$	0.414
p+Au	14.6	$0.11 \pm 0.02$	$0.20 \pm 0.06$	$0.2 \pm 0.1$	1.227
Au+Au	11.6A	$0.502 \pm 0.005$	$0.065 \pm 0.005$	$-0.020 \pm 0.01$	1.381

The rapidity distributions of positive and negative kaons in Pb + Pb collisions at 160 AGeV are calculated in accordance with the SCM, the DBM and the HSD. They are plotted in Figs. 7 and 8 against the experimental background. Furthermore, in the presented plots given in Figs. 9 to 14, we compare the performances of these three models, i.e., the SCM, the BDM and the HSD approach with regard to the

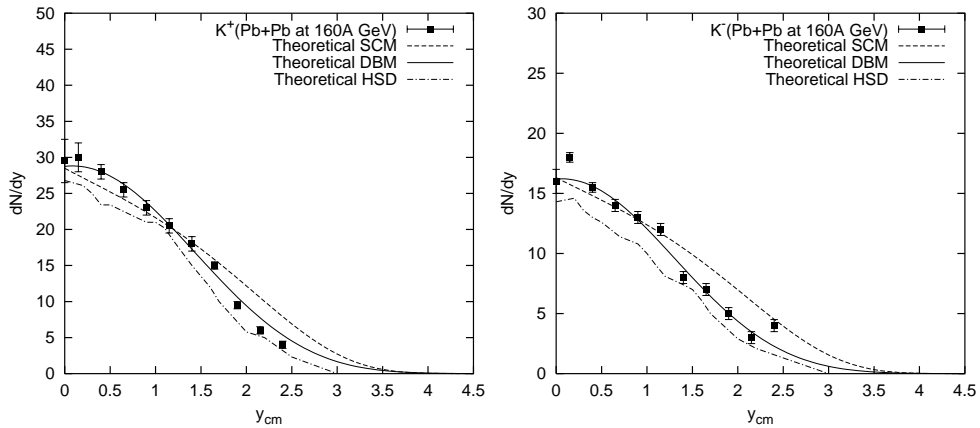


Fig. 7. Rapidity distribution for positive kaons in central Pb + Pb collisions at 160 AGeV/c [6]. The lines show the results of SCM, DBM and HSD model.

Fig. 8 (right). Rapidity distribution for negative kaons in central Pb + Pb collisions at 160 AGeV/c [6]. The lines show the results of SCM, DBM and HSD model.

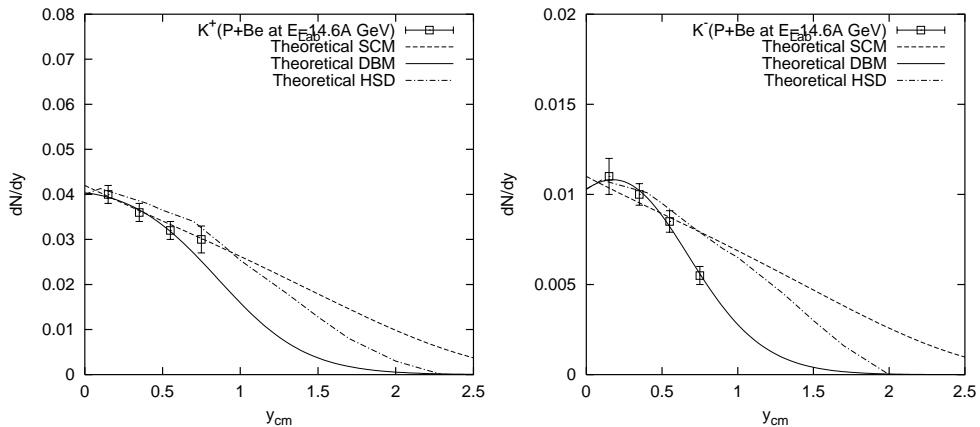


Fig. 9. Rapidity distribution for positive kaons in central p + Be collisions at 14.6 AGeV/c [8,14], i.e., at the AGS energy. The lines show the results of SCM, DBM and HSD model.

Fig. 10 (right). Rapidity distribution for negative kaons in central p + Be collisions at 14.6 AGeV/c [8,14]. The lines show the results of SCM, DBM and HSD model.

$K^+$  and  $K^-$  rapidity distributions separately for  $p + \text{Be}$ ,  $p + \text{Au}$ , both at 14.6 AGeV and  $\text{Au} + \text{Au}$  collisions at 11.6 AGeV against the experimental results.

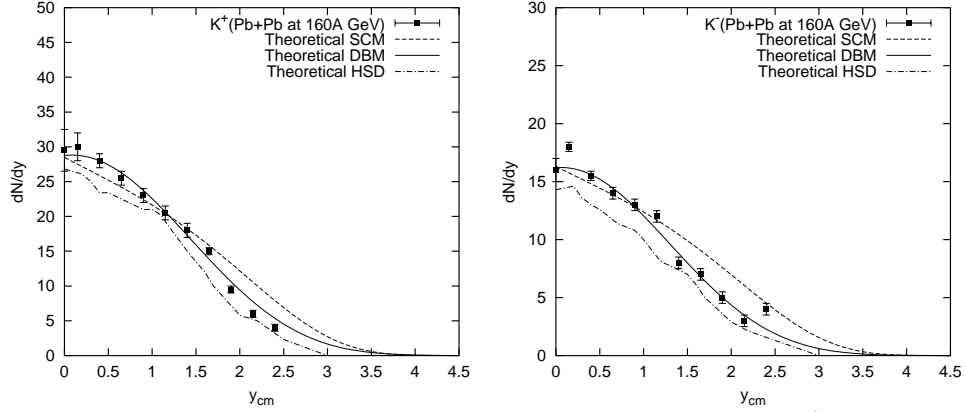


Fig. 11. Presentation of the plot of the rapidity distribution of  $K^+$  for  $p + \text{Au}$  collisions for various values of  $y$ , the rapidity variable at 14.6 AGeV/c. The results of SCM, DBM and HSD approach are shown by the lines against the obtained data sets [8,14].

Fig. 12 (right). Presentation of the plot of the rapidity distribution of  $K^-$  for  $p + \text{Au}$  collisions for various values of  $y$ , the rapidity variable at 14.6 AGeV/c. The results of SCM, DBM and HSD approach are shown by the lines against the obtained data sets [8,14].

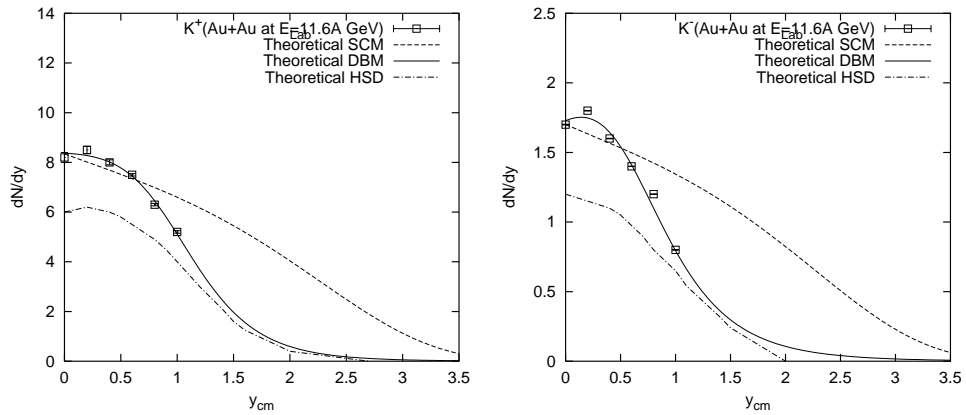


Fig. 13. Presentation of the plot of the rapidity distribution of  $K^+$  for  $\text{Au} + \text{Au}$  collisions for various values of  $y$ , the rapidity variable at 11.6 AGeV/c. The results of SCM, DBM and HSD approach are shown by the lines against the obtained data sets [8,14].

Fig. 14 (right). Rapidity distribution for negative kaons in central  $\text{Au} + \text{Au}$  collisions at 11.6 AGeV/c [8,14]. The lines show the results of SCM, DBM and HSD model.

The state of agreement or disagreement would be discussed in some detail in the next section.

### 3.3. Comparison of $K/\pi$ ratios: data vs. models

#### 3.3.1. High energy sector

In this subsection, we would like to present the calculated results in tabular forms and also in graphical plots. The theoretical results are based on the three models: one set is based on the SCM, another on the DBM and the third on a hydrodynamical model. Prior to this, we make a study on the nature of  $K/\pi$  ratios presented in a previous work [15] with the SCM alone. Now the canvas is wider as there are three models. The SCM-based relation for these figures would be [15]

$$\frac{K}{\pi} = 4.5 \times 10^{-2} (AB)^\alpha (\sqrt{s})^{0.1}, \quad (15)$$

for  $\sqrt{s} \geq 10$  GeV. The parameter  $\alpha$  depends on the nature of the system and it is certainly less than unity.

Let us first present two figures (Figs. 15 and 16) where the nature of kaon to pion ratio in pp and  $p\bar{p}$  collisions are given. The experimental data in Fig. 15 are taken from Ref. [20]. Lines are drawn here from the theoretical calculations of the SCM and the HSD approach. Figure 16 shows strikingly the nature of rise of  $K/\pi$  ratio in the light of SCM only for  $p\bar{p}$  collider at high energies (Ref. [17]).

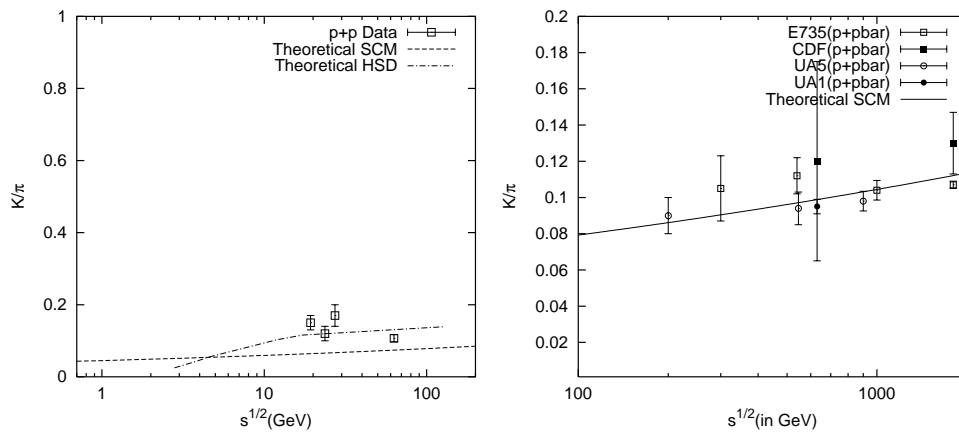


Fig. 15. Presentation of plot of  $K/\pi$  at different centre-of-mass energy for  $p + p$  collisions. The lines indicate the SCM- and HSD-based results against the data sets taken from Ref. [22]

Fig. 16 (right). Presentation of plot of  $K/\pi$  at different centre-of-mass energies for  $p + \bar{p}$  collisions. The solid line indicates the SCM-based results against the data-sets taken from Bocquet et al. [17].

Next, we would like to compare the experimental data and model-based theoretical predictions by the SCM and the HSD of  $K^+/\pi^+$  ratio at RHIC Au + Au collisions in  $\sqrt{s} = 130$  GeV. The data are taken from Ref. [21]. Unfortunately, we are unable to give any theoretical prediction of  $K/\pi$  ratio by DBM at RHIC energy as the complete data of inclusive cross-sections for kaons are not available, and also because of the limitation that the model, uptilnow, is devoid of predictive power.

Hereafter, we are going to present a few tables (Table 5 to Table 7), wherein comparisons of  $K/\pi$  ratios between any pair of the models, viz. the SCM, the DBM and the HSD approach, are made for several nuclear collisions at different energy levels, i.e., at RHIC, SPS and AGS, against experimental background. Moreover, Fig. 17 shows the predictions for kaon-pion ratios by the three chosen models in the energy range from AGS to RHIC. The experimental data are taken for Au + Au collisions at four AGS energies [19], for Pb + Pb collisions at SPS energy

TABLE 5. Strangeness at RHIC energy  $\sqrt{s} = 130$  GeV. Comparison of  $K^+/\pi^+$  ratio obtained by the theoretical SCM and HSD with the measured data taken from Ref. [21].

System	Energy	$\frac{K^+}{\pi^+} _{\text{data}}$	$\frac{K^+}{\pi^+} _{\text{SCM}}$	$\frac{K^+}{\pi^+} _{\text{DBM}}$	$\frac{K^+}{\pi^+} _{\text{HSD}}$
Au+Au	$\sqrt{s}=130$ GeV	$0.169 \pm 0.02$	0.167	–	0.225

TABLE 6. Strangeness at SPS energies: Comparison of the  $\langle K \rangle / \langle \pi \rangle$  ratios obtained by the theoretical SCM, DBM and HSD approaches with measured data taken from NA49 Collaboration [5,18].

Systems	$\frac{\langle K \rangle}{\langle \pi \rangle} _{\text{data}}$	$\frac{\langle K \rangle}{\langle \pi \rangle} _{\text{SCM}}$	$\frac{\langle K \rangle}{\langle \pi \rangle} _{\text{DBM}}$	$\frac{\langle K \rangle}{\langle \pi \rangle} _{\text{HSD}}$
p+p	$0.08 \pm 0.02$	0.06	0.08	0.08
S+S	$0.15 \pm 0.015$	0.15	0.07	0.139
S+Au	$0.13 \pm 0.015$	0.14	–	0.132
Pb+Pb	$0.14 \pm 0.02$	0.14	0.15	0.15

TABLE 7. Strangeness at AGS energies: Comparison of the measured  $\langle K^+ \rangle / \langle \pi^+ \rangle$  yields for different systems at AGS energies with those obtained by the SCM, DBM and HSD approaches within the SCM and HSD approaches. [Data source – E802 Collaboration [8]].

Systems	$\frac{\langle K^+ \rangle}{\langle \pi^+ \rangle} _{\text{data}}$	$\frac{\langle K^+ \rangle}{\langle \pi^+ \rangle} _{\text{SCM}}$	$\frac{\langle K^+ \rangle}{\langle \pi^+ \rangle} _{\text{DBM}}$	$\frac{\langle K^+ \rangle}{\langle \pi^+ \rangle} _{\text{HSD}}$
p+Be	$0.059 \pm 0.01$	0.064	0.07	0.059
Si+Al	$0.12 \pm 0.01$	0.10	–	0.071
Si+Au	$0.17 \pm 0.02$	0.13	–	0.084
Au+Au	$0.18 \pm 0.01$	0.097	0.090	0.095

( $E_{lab} = 160$  AGeV) [6] and for Au + Au at RHIC energy ( $\sqrt{s} = 130$  GeV) [21]. Figures 18 and 19 depict the theoretical curves predicted by the SCM for S + S and

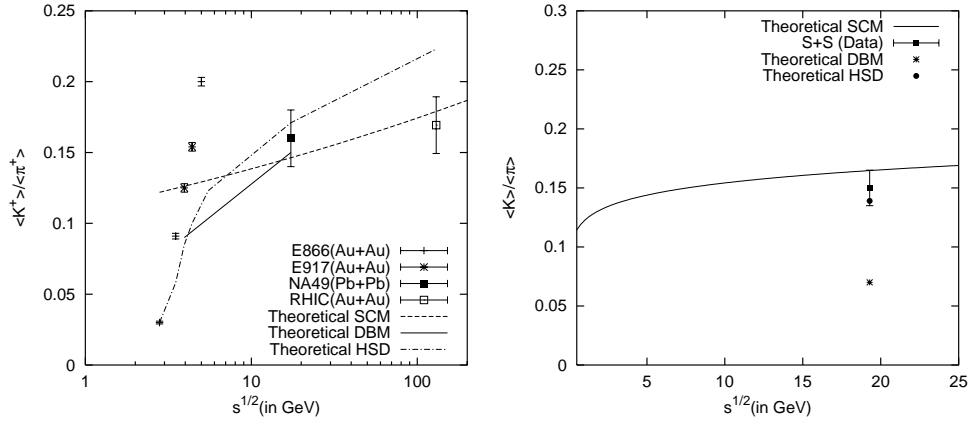


Fig. 17. Nature of  $K^+/\pi^+$  of Au + Au collisions at AGS energies, Pb + Pb collisions at SPS energies and Au + Au at RHIC data are from Refs. [6,19,21]. Also show the theoretical predictions in the light of the SCM, DBM and HSD model.

Fig. 18 (right). Nature of the very slow rise of secondary  $K/\pi$  in the S + S collisions as predicted by the SCM with c.m. energy. Data point is from Ref. [5]. Also shown are the theoretical DBM- and HSD-predicted values.

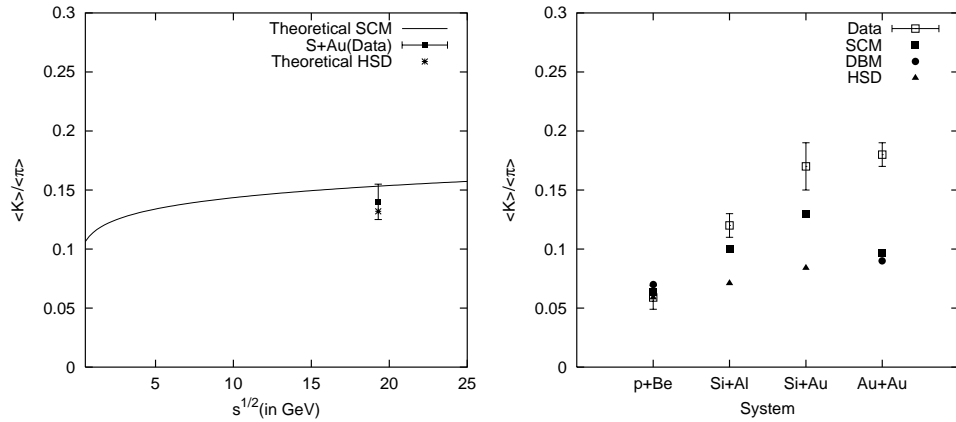


Fig. 19. The SCM-based predicted nature of the  $K/\pi$  for S + Au collisions with c.m. energies. Data point is from Ref. [5]. Also shown is the theoretical HSD-predicted value.

Fig. 20 (right). The  $\langle K^+ \rangle / \langle \pi^+ \rangle$  ratios at AGS energies for p + Be, Si + Al, Si + Au and Au + Au collisions. Data points are from Ref. [8]. Comparison of the SCM, DBM and HSD model are also shown in the picture.

S + Au collisions at 200 AGeV/c. The data-points of each curve are taken from Ref. [5]. Besides, the values attended by both the HSD and DBM are shown by the appropriate symbols in Fig. 18. And the result obtained by only the HSD approach is shown in Fig. 19 by a cross mark, as DBM calculations are still not available on the specific reaction due to the lack of necessary data on certain related and necessary aspect. The results given in Table 7 are also shown in Fig. 20.

### 3.3.2. Relatively lower energy data and the SCM

It is of some interest to probe, quite realistically and on a sampling basis, how the models behave vis-a-vis the relatively lower energy data. Generally valid is the observation that the models which explain data for energies beyond  $s^{1/2} \geq 10$  GeV fail to address the issues at lower energy domain. Among the chosen models here, the SCM is quite plagued with this difficulty, as the model has some inherent high energy assumptions and is based on some approximations which are correct only at very high energies. Or, for its validation, some correction factors need to be operated on the generalised formulae [given here by Eqs. (1) to (6)]. For lower energies,  $\sqrt{s} \leq 10$  GeV, the first correction factor to be applied on Eq. (15) is a multiplier factor of 0.47 arising out of (i) parametrisation for c.m.energy and (ii) the varieties of secondary K-mesons ( $K^+$ ,  $K^-$ ,  $K^0$ ,  $\bar{K}^0$ ). The experimental data are from Pantuev et al. [22] and Laue et al. [23]. The comparisons between theory and measurements are made in the adjoining tables (Tables 8 and 9). The calculated results presented in Tables 8 and 9 are displayed in Fig. 21 and Fig. 22.

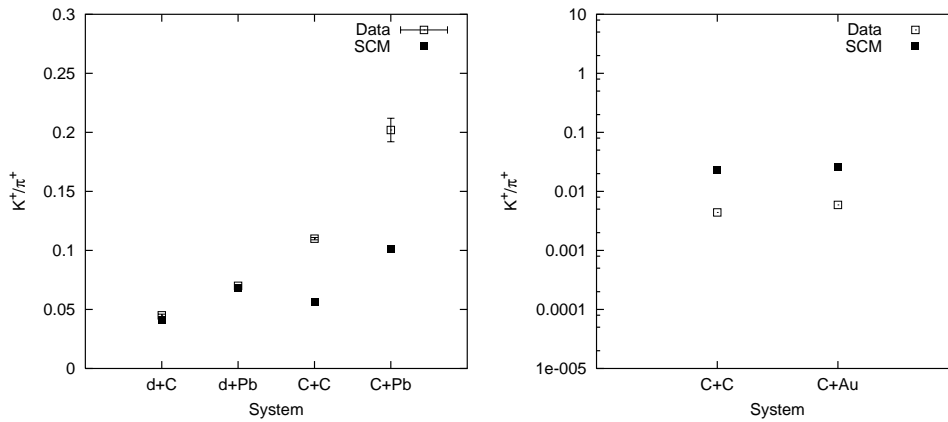


Fig. 21. The SCM-based predicted nature of the  $K/\pi$  for d + C, d + Pb, C + C and C + Pb collisions at 3.65 GeV/nucleon. Data points are taken from Ref. [22].

Fig. 22 (right). The SCM-based predictions of the  $K/\pi$  for C + C and Co + Au collisions at energy 1.8 AGeV. The open squares represent the experimental data-points [23], while the filled squares provide the SCM-based results.

TABLE 8.  $K^+/\pi^+$  production in different relativistic ion collisions at 3.65 GeV/nucleon [Data source Ref. [22]].

Systems:	d+C	d+Pb	C + C	C+Pb
Data:	0.045±0.001	0.07±0.001	0.11±0.001	0.202±0.01
SCM Prediction	0.041	0.068	0.0567	0.101

TABLE 9.  $K^+/\pi^+$  production in two relativistic ion collisions at 1.8 AGeV [Data source Ref. [23]].

Systems	C + C	C + Au
Data	$4.4 \times 10^{-3}$	$5.9 \times 10^{-3}$
SCM Prediction	$2.3 \times 10^{-2}$	$2.6 \times 10^{-2}$

#### 4. General observations and discussion of the results

Let us first make some general observations and specific comments on the results arrived at and shown by the diagrams presented in the figures [Figs. 1 to 19] on a case-to-case basis with regard to the production of a specific secondary in a particular collision at a definite energy. The measures of the rapidity density observables obtained on the basis of the three chosen models, viz. the SCM, the DBM and the HSD, in various nuclear collisions for pion production, at relatively high energies, are depicted in Figs. 1 to 6. They either describe data with modest degree of success, or indicate some incompatibility with data (and, at times, also with each other), with the exception of the case of p + Au (Fig. 2) interactions wherein the SCM offers the most brilliant agreement and the HSD fails to perform satisfactorily. Even for the collision between the heaviest nuclei (Pb + Pb), the models are fairly satisfactory (Fig. 6). However, for the same observable in cases of  $K^+$  and  $K^-$  production of secondaries in several proton-induced or nucleus-induced nuclear collisions (Figs. 7 to 14), the scenario is not so uniform and encouraging for any of the models, especially at relatively lower range of energies. Having judged the performance on an overall and comparative basis, the DBM reproduces the data on kaon production in nuclear reactions most successfully, excepting the cases of pure hadronic collisions. It is to be noted that the DBM is applicable for only the nuclear collisions. Next comes the role of SCM, while the performance by the HSD model is the least satisfactory. But two points must categorically be made on the SCM and the DBM. One of the features of the SCM is: the validity of the model is based on some stringent assumptions on high-energy approximation for which the model works quite well only beyond  $\sqrt{s} \simeq 10$  GeV. And the DBM has an intrinsic weakness in the fact that the model still lacks in predictive capability on all non-pion secondaries, which is an important criterion for any prospective and powerful model. But this inability could be attributed to the lack of reliable and sufficient data on the non-pion varieties of secondaries.

The  $K/\pi$  ratios are presented in Figs. 15 to 19 and some specific values of ratio have been depicted in the tables (Tables 5 to 9). The values of  $K/\pi$  ratios in pp collisions (Fig. 15), derived on the basis of the SCM, show a uniform extremely slow rise, though the absolute values lie much lower than data. This is presumably due to the fact that the SCM is reasonably found to be valid at much higher energies. The role of HSD vis-a-vis data is also shown in Fig. 15 which shows no specific character as such, though within the narrow range of the energy the agreement is much better.

The SCM model offers an excellent fit to the data on  $K/\pi$  ratios at all collider energies (Fig. 16). But we cannot check data on  $p\bar{p}$  collider energies with the two other models, because the natures of energy dependences in these two models are still not explicitly known. In Fig. 17, we present a comparison of all the three models with regard to analysis of data on  $K/\pi$  ratios in the gold-gold and lead-lead collisions at different energies, i.e., from AGS to RHIC energies. The predictivity on the behaviour of the  $K/\pi$  ratios in the light of SCM alone has been shown for the S + S and S + Au collisions at SPS energies in the last two figures (Figs. 18 and 19).

The SCM model is modestly valid for c.m. energy values beyond 10 GeV ( $\sqrt{s} > 13$  GeV), as the model inducts some high-energy approximations on a very stringent basis. Even with a somewhat changed and realistic parametrisation of the same form, the values naturally fall short of the experimentally measured ones given in [22] and [23]. This constraint and inflexibility of the model comes somewhat in an in-built manner for which one is advised not to use it with any parametrisation whatsoever near or below the value 1 GeV of  $\sqrt{s_{NN}^{cm}}$ .

Quite logically, at the lower range of energies, in the region  $\sqrt{s} \leq 10$  GeV, the model(s) behave(s) somewhat erratically. For example, with SCM we could satisfactorily explain the data for the deuteron-induced two collisions, whereas the same model fails to reproduce data on two carbon-induced collisions (Table 8). At still lower energies, at  $E_{Lab} = 1.8$  GeV, the model fails consistently to catch the theoretical prediction, it is roughly one order of magnitude higher than the measured values (Table 9).

## 5. Concluding remarks

Let us now summarise the conclusions from the analyses of the results given above which reflect and reveal the undermentioned realities through the following statements:

(i) In explaining the rapidity density for production of pions (Figs. 1 to 6), the majority of the produced secondaries, the SCM works quite agreeably with data. In our rating, it performed either at par with or better than the DBM and the HSD, both phenomenological models so far. The success of the SCM in describing the rapidity density in different collisions at several high energies available so far is also the central theme of one of our previous works [24].

(ii) With regard to kaon production (inclusive of both charged varieties) (Figs.

7 to 14), however, there is a reversal of faces: the DBM appears to cater to the data-sets in the most agreeable manner, whereas the other two models lag behind. Still, the SCM is comparatively better than the HSD in most cases.

(iii) The agreement between the measured data on  $K/\pi$  ratio in  $p + \bar{p}$  reactions and the theoretical SCM plot (shown in Fig. 16) obtained on the basis of expression (15) here (with  $A=B=1$  for  $p + \bar{p}$  collisions) is strikingly encouraging for the future prospects of SCM.

(iv) But, the agreement between the data on kaon-pion ratios and the SCM and HSD models, at AGS and CERN-SPS energies, are just modestly satisfactory. However, in explaining this latter set of data, the SCM performance is visibly better. And this is also confirmed from Fig. 17 where we made a comparison between the three models for the nuclear collisions at AGS, SPS and at RHIC energies.

(v) The basically predictive graphs given in Figs. 18 and 19 could vindicate this point in future. The initial indication by the single data-point is encouraging for the SCM. This is in spite of area of disargeement [Figs. 21 and 22] between SCM-based results and the actual measurements at very low energies as this is natural for the model at such low energies. However, more data from several nucleus-nucleus collisions and at various energies are awaited for further confirmation, if any, of the model.

(vi) Both the SCM and the DBM can and do explain the full range of the data-sets here on the rapidity density observables without any reckoning of the complications arising out of the rescattering and cascading effects. These two factors are normally discussed with a high degree of seriousness against the background of theoretical/phenomenological studies on the behaviour of high energy nuclear collisions. For the HSD approach, however, these effects need to be incorporated in calculations in a compulsory way, especially for strangeness production. These traits give SCM and BDM an edge over the HSD approach, in so far as the present work is concerned.

(vii) Let us now just extrapolate the preceding point and make an extension. In view of the totality of the work done here, we are finally in a position to raise a very pertinent and provocative question: is there really a need in describing the features of nuclear collisions to employ re-scattering and cascading effects to describe the features of particle yields in high energy nuclear collisions? The question specially springs from the observations that, at least, one of the models (SCM here) can explain the characteristics without introduction of these effects. So, the role and the real need for these much-talked-about effects come under the shades and, thus under doubtful status.

(viii) The checking of relatively lower energy data on some nuclear collisions with the models generally valid for very high energies leads, once again, to the affirmation of the two-sector approach towards theorisation of particle and nuclear interactions.

A comment is in order here. True, on the behaviour of  $K/\pi$  ratios, we did not differentiate here precisely between what is known as “global (g) kaon-to-pion ( $R_g = \langle K \rangle / \langle \pi \rangle$ ) ratio” and what goes by the name of “event-by-event” (ev) ratio

of kaon to pion, represented symbolically by  $R_{ev} = K/\pi$ . According to the philosophy of the event-by-event analysis [25], it is correct that the conditions to produce conjectured QGP might be reached in every event; but the fact that a phase transition is a critical phenomenon implies immediately that it may occur in a small sub-sample of events. The fluctuations in such events would be averaged out in the conventional ensemble analyses. In contrast, the event-by-event analysis, which became possible only with the advent of the large acceptance detectors (LADs), helps us to find or sort out the very interesting or anomalous event candidates with some specific dynamical properties. So, this event-by-event method could provide dynamical information which is not available from the analysis of traditional inclusive spectra or just average multiplicity.

The limitations of the present work are, thus, as follows: (a) We have not reckoned here with the aspects of either the statistical or the dynamical fluctuations. (b) There is no correlation of any kind between the two types of particles viz.,  $\pi$ -mesons and K-mesons. (c) So, on extrapolation of (a) and (b) here, one has to admit that the present study fails to throw light on the questions posed by Yang and Cai [25]. This is surely a limitation of this work.

#### *Acknowledgements*

The authors would like to express their gratitude to the two anonymous learned referees for their helpful suggestions and constructive criticisms of the earlier draft of the manuscript. It is also a pleasure to acknowledge very deeply the kind help received from Prof. M. M. Aggarwal of Dept. of Physics, Punjab University and Prof. I. Seldrup of IJMPE who were kind enough to send us a reprint necessary for completing this work. One of the authors, PGR, is grateful to the UGC (INDIA) for its financial support through the Faculty Development Programme.

### **Appendix: The approximate estimation of $dN/dy$ in central rapidity region for nucleus-nucleus collisions**

We proceed in the route built up by Wong [10] to bridge the gap between nucleon-nucleon and nucleus-nucleus collisions.

Let us consider nuclear reaction  $A + B \rightarrow C + X$ , where A and B are projectile and target nucleus respectively. For two unequal nuclei, the relationship between the rapidity distributions for nucleus-nucleus and nucleon-nucleon collisions would be

$$\left. \frac{dN}{dy} \right|_{AB} \simeq 1.28 \frac{AB}{A^{2/3} + B^{2/3}} \frac{1}{1 + a(A^{1/3} + B^{1/3})} \times \exp\left(-\frac{b^2}{2\beta^2}\right) \left. \frac{dN}{dy} \right|_{pp} \quad (16)$$

where  $a$  is the parameter that is to be chosen and  $b$  is the impact parameter. The term  $\beta^2$  satisfies the following relation:  $\beta^2 = \beta_A^2 + \beta_B^2 + \beta_p^2$ . Here,  $\beta_A = r'_0 A^{1/3} / \sqrt{3}$  with  $r'_0 = 1.05$  fm, and  $\beta_p$ , the thickness function parameter for nucleon - nucleon collisions, is 0.68 fm.

For two equal nuclei, the relation would then become

$$\left. \frac{dN}{dy} \right|_{AB} \simeq 0.64 A^{4/3} \frac{1}{1 + 2aA^{1/3}} \exp\left(-\frac{b^2}{2\beta^2}\right) \left. \frac{dN}{dy} \right|_{pp}. \quad (17)$$

For unequal nuclei,  $(dN/dy)_{AB}$  just reduces to,

$$\left. \frac{dN(b)}{dy} \right|_{\text{peak}} \simeq 1.28 \frac{AB}{A^{2/3} + B^{2/3}} \frac{1}{1 + a(A^{1/3} + B^{1/3})} \times \exp\left(-\frac{b^2}{2\beta^2}\right) \left. \frac{dN_{pp}}{dy} \right|_{\text{peak}}. \quad (18)$$

#### References

- [1] J. I. Kapusta, J. Phys. G **27** (2001) 593. S. E. Vance, J. Phys. G **27** (2001) 603.
- [2] C. Sturm et al., Phys. Rev. Lett. **86** (2001) 39.
- [3] D. E. Kahana and S. H. Kahana, Phys. Rev. C **63** (2001) 031901R.
- [4] M. M. Agarwal and S. A. Garpman, Int. J. Mod. Phys. E, **4** (1995) 477.
- [5] C. Bormann et al. (NA49 Collaboration), J. Phys. G **23** (1997) 1817.
- [6] F. Sikler et al. (NA49 Collaboration), Nucl. Phys. A **661** (1999) 45c.
- [7] T. Alber et al. (NA35 Collaboration), Phys. Lett. B **366** (1996) 56.
- [8] Ahle et al. (E802 Collaboration), Nucl. Phys. A **610** (1996) 139c.
- [9] (a) S. Bhattacharyya, J. Phys. G **14** (1988) 9; (b) S. Bhattacharyya, Il Nuovo Cimento C **11** (1988) 51. (c) P. Bandyopadhyay and S. Bhattacharyya, Il Nuovo Cimento A **43** (1978) 305.
- [10] C. Y. Wong, *Introduction to High Energy Heavy Ion Collisions*, World Scientific, Singapore (1994).
- [11] B. De, S. Bhattacharyya, Eur. Phys. J. A **10** (2001) 387; Bhaskar De and S. Bhattacharyya, Mod. Phys. Lett. A **16** (2001) 1395.
- [12] Bhaskar De, P. Guptaroy and S. Bhattacharyya, to appear in Int. J. Mod. Phys. A (2002).
- [13] N. Thome et al., Nucl. Phys. B **129** (1977) 365.
- [14] J. Geiss, W. Cassing and C. Greiner, Nucl. Phys. A **644** (1998) 107; W. Cassing, E. L. Bratkovskaya and S. Juchem, nucl-th/0001024.
- [15] S. Bhattacharyya, B. De, P. Guptaroy and D. P. Bhattacharyya, Had. J. (Suppl.) **15** (2000) 451.
- [16] J. Bachler et al., Nucl. Phys. A **661** (1999) 45c.
- [17] G. Bocquet et al., Phys. Lett. B **366** (1996) 447.
- [18] D. Rohrich, J. Phys. G **27** (2001) 355.
- [19] B. B. Back et al., J. Phys. G **27** (2001) 301.
- [20] D. Antreasyan et al., Phys. Rev. D **19** (1979) 764; K. Guettler et al., Nucl. Phys. B **116** (1976) 77.
- [21] P. Braun-Munzinger et al., Phys. Lett. B **518** (2001) 41.

- [22] V. S. Pantuev et al., Nucl. Phys. A **585** (1995) 13c.
- [23] F. Laue et al., Eur. Phys. J. A **9** (2000) 397.
- [24] P. Guptaroy, Bhaskar De, S. Bhattacharyya and D. P. Bhattacharyya, Heavy Ion Physics **15** (2002) 103.
- [25] C. B. Yang and X. Cai, Int. J. Mod. Phys. A **16** (2001) 1227.

#### MNOGOBROJNA TVORBA PIONA I KAONA U VISOKOENERGIJSKIM SUDARIMA JEZGRA-JEZGRA: ISHODI MJERENJA I POSEBNI MODELI

Gustoće rapidnosti piona i kaona i narav omjera kaona i piona pružaju dvije vrlo važne fizičke opservable za koje su dosada postignuti brojni podaci mjerenjem sudara teških jezgri. Ispitujemo skladnost teorije polazeći od dva skupa modela, jednog potpuno fenomenološkog i drugog s umjerenim stupnjem dinamike, i eksperimentalnih podataka poznatih iz ranijih i nedavnih mjerenja. Raspravlja se njihova važnost i sljedbe.